Impact Ionization Model Using Average Energy and Average Square Energy of Distribution Function

Ken-ichiro SONODA*, Scott T. DUNHAM[1], Mitsuru YAMAJI, Kenji TANIGUCHI and
Chihiro HAMAGUCHI

Department of Electronic Engineering, Osaka University, Yamada-oka, Suita, Osaka 565, Japan
[1]*Department of Electrical, Computer, and Systems Engineering, Boston University, 44*
Cummington Street Boston, Massachusetts 02215, U.S.A.

Abstract

A new impact ionization model is developed using both the average energy and the average square energy of electrons. The accuracy of the model in an inhomogeneous electric field is verified through comparison with results calculated with Monte Carlo simulation. Our model predicts the generation rate even in an inhomogeneous field more accurately than local field, non-local field, and local energy models.

1. Introduction

Recent progress in manufacturing technology has made it possible to fabricate deep submicron semiconductor devices. However, power supply voltage has not been scaled down in line with the physical dimensions of MOSFETs (metal oxide semiconductor field effect transistors) so that higher circuit performance can be achieved and TTL compatibility maintained. The hot carrier effect due to a high electric field in the scaled-down devices, which causes device degradation, has been the main concern in recent years. The presence of large field gradient and the multi-dimensional nature of the physical phenomena make it difficult to analyze hot carrier effects in MOSFETs.

In a homogeneous electric field, E, the impact ionization (I.I.) coefficient, α, i.e., the number of ionization events per unit length along a current path, obeys Chynoweth's law,[1] $\alpha \propto \exp(-E_c/E)$, which is derived from a lucky electron model.[2] In a homogeneous field, the applied electric field determines the electron distribution function, and therefore, α can be expressed as a unique function of E. α determined by a local electric field is called as a local field (LF) model.

In the case of the electric field varying within the energy relaxation length, $v_{\mathrm{sat}}\tau_{\langle\varepsilon\rangle}$ ($\sim 0.05\mu$m), the energy distribution function is not well described with the local electric field; the ionization coefficient is no longer expressed by the local electric field alone and the I.I. is "non-local." The LF model overestimates the ionization coefficient in increasing electric field. In order to overcome this shortcoming, a non-local field (NLF) model[3–5] was proposed. In

---

*On leave from ULSI Laboratory, Mitsubishi Electric Corporation, Mizuhara, Itami, Hyogo 664, Japan.

the model, carrier trajectories are traced back along the electric field path to a point where the electrostatic potential difference is equal to an effective threshold energy for impact ionization, V_{I}. The ionization coefficient is expressed in terms of the path length d as $\alpha \propto \exp(-d/\lambda_{\mathrm{p}})$,[5] where λ_{p} is an effective mean free path without being scattered with optical phonons. In a homogeneous field, the model reduces to the LF model with the relation $\lambda_{\mathrm{p}} = V_{\mathrm{I}}/E_{\mathrm{c}}$. In this method, the I.I. phenomenon is treated as a one-dimensional problem. In reality, high-energy electrons move around in three-dimensional space so that the application of this method to multi-dimensional problems is questionable.

The exact calculation of impact ionization coefficient requires the use of a high energy distribution function because impact ionization events are caused by energetic carriers.

The average energy of the distribution function is the basic parameter with which to characterize the energy distribution. Therefore, it is more appropriate to use average energy rather than an electric field to express the impact ionization coefficient. In a homogeneous high electric field, the average energy, $\langle\varepsilon\rangle$, is given by the electric field, E, as $\langle\varepsilon\rangle = qEv_{\mathrm{sat}}\tau_{\langle\varepsilon\rangle}$. This relationship is combined with a local field model to give

$$\alpha \propto \exp\left(-\frac{\varepsilon_{\mathrm{c}}}{\langle\varepsilon\rangle}\right). \tag{1}$$

This model is called the local energy (LE) model because the ionization coefficient is expressed as a function of local average energy. The critical energy ε_{c} is obtained from $\varepsilon_{\mathrm{c}} = qE_{\mathrm{c}}v_{\mathrm{sat}}\tau_{\langle\varepsilon\rangle}$. This model is often used in the hydro-dynamic and energy transport models[6–8]. Although other expressions for the impact ionization generation rate have been proposed,[9–11] all are expressed as a function of average energy.

Recent Monte Carlo simulations[12–14] showed that in an inhomogeneous field, average energy is still insufficient to estimate the impact ionization generation rate; the average energy is not an appropriate measure of the impact ionization rate. Several attempts have been made to improve the accuracy of the high-energy population of the distribution function by solving conservation equations for the high-energy tail.[13,14] However, some ambiguity remains in defining the boundary conditions between the low-energy and high-energy regimes.

We propose an impact ionization model formulated using both the average energy and the average square energy of the distribution function for more precise description of impact ionization.

2. Physical Models

A. Distribution functions

It is well known that the microscopic impact ionization probability depends on the wave vectors of primary electrons. The anisotropy of impact ionization near the threshold energy of 1.1eV arises due to the complex band structure of silicon. In the energy range above 2.5eV, where most impact ionization events occur, the probability is almost isotropic.[15–18] Below, we assume that both the distribution function and the impact ionization probability are isotropic in the energy range of interest.

The energy distribution function, f, can be characterized by its moments:

$$n = \int f d\boldsymbol{k} \tag{2}$$

$$n\langle\varepsilon^i\rangle = \int f\varepsilon^i d\boldsymbol{k} \qquad (i = 1, 2, \ldots). \tag{3}$$

Although the distribution function cannot be uniquely determined by a finite number of moments, it is reasonable to assume that the distribution function has maximum entropy under a given number of the moments. The entropy, S, of the distribution function, f, is defined as

$$S = \int f(1 - \log f) d\boldsymbol{k}. \tag{4}$$

Using the variational method of Lagrange multipliers, the distribution function with maximum entropy is given by[19]

$$f = \exp\left\{\sum_{i=0}^{N} a_i\varepsilon^i\right\}. \tag{5}$$

a_i's are determined to satisfy the moments defined by eqs. (2) and (3). If $N = 1$, meaning that both a carrier concentration and an average energy are given, eq. (5) becomes the Maxwell-Boltzmann distribution.

Since the impact ionization rate in an inhomogeneous electric field[12–14] is not a unique function of average energy, we utilize a higher-order moment, $\langle\varepsilon^2\rangle$, as an additional measure to formulate the I.I. rate.

When $\langle\varepsilon\rangle$ and $\langle\varepsilon^2\rangle$ are given, the distribution function with maximum entropy is given by

$$f = \exp(a_0 + a_1\varepsilon + a_2\varepsilon^2). \tag{6}$$

The variables, a_0, a_1, and a_2, are determined as

$$n = \int D f d\varepsilon \tag{7}$$

$$n\langle\varepsilon\rangle = \int D f \varepsilon d\varepsilon \tag{8}$$

$$n\langle\varepsilon^2\rangle = \int D f \varepsilon^2 d\varepsilon, \tag{9}$$

where D is the density of states. The numerical procedure to obtain the values of these variables is shown in the appendix.

The Monte Carlo simulator used in this study features multi-analytical valleys to express the band structure of silicon. The parameters for describing the structure of the valleys are calibrated to fit the density of states up to 5eV to the one calculated by a pseudo-potential method.[20] Scattering models implemented in the program are (1) acoustic and optical phonon scatterings calculated using a rigid pseudo-ion model,[20] and (2) impact ionization with an analytical form[17] of $P_{\rm ii} = 1.0 \times 10^{11}\,(\varepsilon - \varepsilon_{\rm th})^{4.6}\,{\rm s}^{-1}, \quad \varepsilon_{\rm th} = 1.1{\rm eV}$.

All the physical parameters used in our analytical Monte Carlo simulator are well calibrated with the full-band Monte Carlo simulator[20] so that the calculated drift velocity, average energy and impact ionization coefficient are the same as those obtained from the full-band Monte Carlo simulator.

Figure 1 shows the average energy, $\langle\varepsilon\rangle$, and the normalized average square energy, $\xi = \sqrt{(3/5)\langle\varepsilon^2\rangle}/\langle\varepsilon\rangle$, respectively, calculated using the Monte Carlo simulator in homogeneous electric field.

As shown in Fig. 2(a), the distributions given by eq. (6) well reproduce the calculated results of Monte Carlo simulation. The normalized average square energy approaches the value of $\xi_{\rm h} = 0.88$ asymptotically as the field increases. In the field range above $E > 200$kV/cm where impact ionization events occur frequently, the parameter, ξ, can be regarded as a constant. It should be noted that $\langle\varepsilon\rangle$ is not sufficient to describe the distribution function even in a homogeneous field, as shown in Fig. 2(b).

Figure 3 shows the average energy and normalized average square energy in an inhomogeneous field which increases exponentially and decreases linearly; the field resembles the channel field near the drain of surface channel MOSFETs.[21,22] In the increasing field region, ξ is less than $\xi_{\rm h}$, the value in the homogeneous high field. The distribution function in this region is well expressed by eq. (6), as shown in Fig. 4(a).

In the decreasing field region, ξ exceeds $\xi_{\rm h}$. In this region, the energy distribution function consists of hot electrons generated by the high electric field and cold electrons diffused from the right low-field region, as shown in Figs. 4(b) and 4(c). In the decreasing field region where ξ is larger than $\xi_{\rm h}$, the distribution function can be given by

$$f = f_{\rm cold} + f_{\rm hot}. \tag{10}$$

The following relationships are derived from eq. (10).

$$n = n_{\rm cold} + n_{\rm hot} \tag{11}$$

$$n\langle\varepsilon\rangle = n_{\rm cold}\langle\varepsilon\rangle_{\rm cold} + n_{\rm hot}\langle\varepsilon\rangle_{\rm hot} \tag{12}$$

$$n\langle\varepsilon^2\rangle = n_{\rm cold}\langle\varepsilon^2\rangle_{\rm cold} + n_{\rm hot}\langle\varepsilon^2\rangle_{\rm hot} \tag{13}$$

We further assume that

1. $f_{\rm cold}$ is the Maxwell-Boltzmann distribution with a lattice temperature of T_0, or

$$\langle\varepsilon\rangle_{\rm cold} = \frac{3}{2}kT_0 \tag{14}$$

$$\langle\varepsilon^2\rangle_{\rm cold} = \frac{15}{4}(kT_0)^2; \tag{15}$$

2. $f_{\rm hot}$ is expressed by eq. (6) with the normalized average square energy, $\xi_{\rm h}$ or

$$\langle\varepsilon^2\rangle_{\rm hot} = \frac{5}{3}\xi_{\rm h}^2\langle\varepsilon\rangle_{\rm hot}^2. \tag{16}$$

Equations (11)–(16) yield $n_{\rm cold}/n$, $n_{\rm hot}/n$, and $\langle\varepsilon\rangle_{\rm hot}$ for given $\langle\varepsilon\rangle$ and $\langle\varepsilon^2\rangle$.

The distribution functions calculated from eq. (10) are compared with Monte Carlo results shown in Figs. 4(b) and 4(c), and it is found that eq. (10) well reproduces the distribution function at $\xi > \xi_{\rm h}$.

The distribution function in the inhomogeneous field is, therefore, expressed as

$$f=\begin{cases}\exp(a_0+a_1\varepsilon+a_2\varepsilon^2) & (\xi<\xi_\mathrm{h}:\text{increasing field})\\ f_\mathrm{cold}+f_\mathrm{hot} & (\xi>\xi_\mathrm{h}:\text{decreasing field})\end{cases}. \tag{17}$$

Note that both eq. (6) and eq. (10) give the same result at $\xi=\xi_\mathrm{h}$.

The energy distribution function for electrons given by eq. (6) has been reported.[23] However, it leads to an incorrect result because only the average energy of electrons is used to determine the distribution; the impact ionization rate depends only on the average energy.

B. Impact ionization generation rate

The generation rate due to impact ionization, G_ii, is calculated from

$$G_\mathrm{ii}=\int DfP_\mathrm{ii}d\varepsilon, \tag{18}$$

where P_ii is impact ionization probability, which is well approximated as

$$P_\mathrm{ii}=\begin{cases}0 & (\varepsilon<\varepsilon_\mathrm{th})\\ P_\mathrm{ii\,0}\left(\varepsilon-\varepsilon_\mathrm{th}\right)^r & (\varepsilon>\varepsilon_\mathrm{th})\end{cases}, \tag{19}$$

where $P_\mathrm{ii\,0}=1.0\times10^{11}\mathrm{s}^{-1}\mathrm{eV}^{-r}$, $r=4.6$, and $\varepsilon_\mathrm{th}=1.1\mathrm{eV}$.[17] The impact ionization probability increases gradually above the threshold energy, which indicates a soft threshold.

Substituting eqs. (17) and (19) into eq. (18), one obtains the impact ionization rate as a function of the average energy, $\langle\varepsilon\rangle$, and the average square energy, $\langle\varepsilon^2\rangle$ of electrons.

The numerically calculated generation rate based on eqs. (17)–(19) is shown in Fig. 5. The generation rate depends on both the average energy, $\langle\varepsilon\rangle$, and the normalized average square energy, ξ. The ionization rate obtained from the Monte Carlo simulation in a homogeneous electric field is also shown in the same figure by a dashed curve. The calculated generation rate at $\xi=0.88$ agrees quite well with the Monte Carlo result, which supports the finding that ξ converges to $\xi_\mathrm{h}=0.88$ in a high electric field.

At $\xi=0.88$, the generation rate is expressed as

$$G_\mathrm{ii}=ng_\mathrm{ii\,0}\exp\left(-\frac{\varepsilon_\mathrm{c}}{\langle\varepsilon\rangle}\right), \tag{20}$$

where $g_\mathrm{ii\,0}=1.39\times10^{14}\mathrm{s}^{-1}$ and $\varepsilon_\mathrm{c}=8.78\mathrm{eV}$. The characteristic energy, ε_c, is much larger than the energy band gap of silicon due to the soft threshold nature of impact ionization in silicon.

We empirically express the calculated result as

$$G_\mathrm{ii}=ng_\mathrm{ii\,0}\exp\left(-\frac{\varepsilon_\mathrm{c}}{\langle\varepsilon\rangle_\mathrm{eff}}\right) \tag{21}$$

using the effective energy for impact ionization, $\langle\varepsilon\rangle_\mathrm{eff}$. The effective energy calculated from eq. (21) and G_ii in Fig. 5 are plotted in Fig. 6 as a parameter of the normalized average square energy ξ. It is found that the effective energy can be expressed as a linear function of the average energy, though it depends on the value of ξ.

For $\xi < \xi_{\mathrm{h}}$, the ratio, $\langle\varepsilon\rangle_{\mathrm{eff}}/\langle\varepsilon\rangle$, is less than unity. This means that the "electron temperature" for impact ionization is lower than that given from the average energy. For $\xi > \xi_{\mathrm{h}}$, the "electron temperature" for impact ionization is higher than that from the average energy.

Figure 7 shows that the ratio is a unique function of ξ in the range of our study and is approximated as

$$\frac{\langle\varepsilon\rangle_{\mathrm{eff}}}{\langle\varepsilon\rangle} = \exp(\gamma(\xi - \xi_{\mathrm{h}})), \tag{22}$$

where $\gamma = 4.21$ for $\xi < \xi_{\mathrm{h}}$ and $\gamma = 1.56$ for $\xi > \xi_{\mathrm{h}}$.

The new impact ionization model consists of eqs. (21) and (22) which are expressed as a function of both the average energy and the average square energy.

Note that the new I.I. model contains only local variables. No further assumption about a field profile is made in the derivation process.

3. Results and Discussion

Figure 3 shows the calculated impact ionization rates in the inhomogeneous field using several I.I. models. The models and parameters used are summarized in Table I. These parameters are calibrated to give the same generation rate in a homogeneous electric field. In order to verify the validity of the physical models, the calculated results are compared with the Monte Carlo results, as shown in Fig. 8. In the LF and NLF models, the generation rate is calculated using $G_{\mathrm{ii}} = nv_{\mathrm{d}}\alpha$, where v_{d} is the drift velocity derived from Monte Carlo simulation. The average energy, and the normalized average square energy calculated from Monte Carlo simulation shown in Fig. 3 are used in the LE and our new models.

The LF model overestimates the generation rate by over one order of magnitude in the increasing field region, while it underestimates the generation rate in the decreasing region. The NLF model improves the accuracy in the decreasing field region, as reported in the literature.[5] However, the generation rate in the increasing field region and its maximum value are still too large. The LE model gives a maximum I.I. rate closer to the Monte Carlo result than does the LF or NLF model. This model, however, still overestimates I.I. rate in the increasing field region and underestimates it in the decreasing field region, similar to the LF model. In contrast to the previous three models, our new model shows excellent agreement with the full-band Monte Carlo simulation in both increasing and decreasing field regions. At the point C ($x = 0.69\mu$m) in Fig. 3, the LE model gives a low I.I. rate, as shown in Fig. 8, because of low average energy (0.13 eV). At the same point, the new model well reproduces the I.I. rate derived from Monte Carlo simulation, which suggests that the energy distribution function is properly described by using both an average energy and an average square energy even if it is far from Maxwellian, as shown in Fig. 4(c).

In order to demonstrate the applicability of our new model in the deep submicron regime, we investigate the I.I. rate in steeper electric field profiles. Figure 9 shows the electric profile with $\lambda = 0.05\mu$m and the calculated I.I. rates. The value, $\lambda = 0.05\mu$m, corresponds to typical 0.35μm CMOS technologies (e.g., $t_{\mathrm{ox}} = 75$Å and $x_{\mathrm{j}} = 0.1\mu$m) with the formula

$\lambda = \sqrt{3 t_{\rm ox} x_{\rm j}}$.[24] In this case, the I.I. rate with the new model agrees with the Monte Carlo result within a factor of two. The electron energy distribution functions at points A–C in Fig. 9 are shown in Fig. 10. Note that the analytical expression of eq. (17) well reproduces the distributions obtained from Monte Carlo simulation.

In the case of $\lambda = 0.02\mu$m, a typical 0.1μm n-MOS (e.g., $t_{\rm ox} = 40$Å and $x_{\rm j} = 0.05\mu$m), our model gives an I.I. rate larger by over one order of magnitude than the result obtained from Monte Carlo calculation, as shown in Fig. 11. The discrepancy results because eq. (17) is no longer able to express the plateau distribution functions in Fig. 12 which suggest apparent ballistic transport. Although the new model has rather poor predictability of the I.I. rate for MOSFETs below $L = 0.35\mu$m, it is the only model that predicts the generation rate on the decreasing side of the I.I. rate; other conventional (LF, NLF, and LE) models completely ignore it. Note that the NLF model gives no impact ionization because the total potential drop in Fig. 11 is 1.5 V, which is smaller than the value of the effective threshold energy for impact ionization, $V_{\rm I} = 1.75$ eV,[5] used in this study.

4. Conclusions

We proposed an impact ionization model which was formulated using the average energy and the average square energy of electrons. This model was derived from a distribution function which maximizes the entropy of the distribution. The calculated result using the new model well reproduced the impact ionization rate calculated from Monte Carlo simulation in both increasing and decreasing field profiles which always exists for MOSFETs operating at high voltage. The new impact ionization model was shown to be applicable down to 0.35μm n-MOSFETs.

Acknowledgements

One of the authors (K. S.) thanks Dr. N. Kotani of ULSI Laboratory, Mitsubishi Electric Corporation for his encouragement and constant support. This work was partially supported by the Ministry of Education, Science, Sports, and Culture under Grant-in-Aid for Scientific Research on Priority Areas, "Ultimate Integration of Intelligence on Silicon Electronic Systems."

Appendix: Numerical Procedure to obtain a_0, a_1, and a_2

We define the i-th moment, M_i, of the distribution function, f,

$$f = {\rm e}^{a_0 + a_1 \varepsilon + a_2 \varepsilon^2}, \tag{23}$$

as

$$M_i \equiv \int D f \varepsilon^i d\varepsilon. \tag{24}$$

The distribution function, f, is assumed to be normalized as $\int D f d\varepsilon = 1$.

The equation to be solved is

$$\boldsymbol{F}(\boldsymbol{a}) = \quad , \tag{25}$$

where

$$\boldsymbol{F} \equiv \begin{bmatrix} F_0 \\ F_1 \\ F_2 \end{bmatrix} = \begin{bmatrix} M_0 - 1 \\ M_1 - \langle \varepsilon \rangle \\ M_2 - \langle \varepsilon^2 \rangle \end{bmatrix} \tag{26}$$

$$\boldsymbol{a} \equiv \begin{bmatrix} a_0 \\ a_1 \\ a_2 \end{bmatrix} . \tag{27}$$

Equation (25) can be solved by Newton's method. The Jacobian of this equation becomes the symmetric matrix

$$\frac{\partial \boldsymbol{F}}{\partial \boldsymbol{a}} = \begin{bmatrix} M_0 & M_1 & M_2 \\ M_1 & M_2 & M_3 \\ M_2 & M_3 & M_4 \end{bmatrix} . \tag{28}$$

The moments M_i's are numerically calculated. The variables a_0, a_1, and a_2 are obtained by solving the linear algebraic equation

$$\frac{\partial \boldsymbol{F}}{\partial \boldsymbol{a}} \delta \boldsymbol{a} = -\boldsymbol{F} \tag{29}$$

and updating the variables

$$\boldsymbol{a} \leftarrow \boldsymbol{a} + \delta \boldsymbol{a} \tag{30}$$

until they converge.

REFERENCES

1. A. G. Chynoweth: Phys. Rev. **109** (1958) 1537.
2. W. Shockley: Solid-State Electron. **2** (1961) 35.
3. T. Thurgate and N. Chan: IEEE Trans. Electron Devices **32** (1985) 400.
4. R. Kuhnert, C. Werner and A. Schütz: IEEE Trans. Electron Devices **32** (1985) 1057.
5. H. J. Peifer, B. Meinerzhagen, R. Thoma and W. L. Engl: IEDM Tech. Dig. (1991) 131.
6. M. Fukuma and W. W. Lui: IEEE Electron Device Lett. **8** (1987) 214.
7. Y. Apanovich, E. Lyumkis, B. Polsky, A. Shur and P. Blakey: IEEE Trans. Computer-Aided Design **13** (1994) 702.
8. V. M. Agostinelli, Jr., T. J. Bordelon, X. Wang, K. Hasnat, C-.F. Yeap, D. B. Lemersal, Jr., A. F. Tasch and C. M. Maziar: IEEE Trans. Electron Devices **41** (1994) 1784.
9. K. Rahmat, J. White and D. A. Antoniadis: IEDM Tech. Dig. (1991) 115.
10. W. Quade, E. Schöll and M. Rudan: Solid-State Electron. **36** (1993) 1493.
11. J. Z. Peng, S. Longcor and J. Frey: IEICE Trans. Electron. **E77-C** (1994) 166.
12. T. Iizuka and H. Kato: 1993 Int. Workshop on Numerical Modeling of Processes and Devices for Integrated Circuits (NUPAD V) (1994) p. 59.
13. J.-G. Ahn, C.-S. Yao, Y.-J. Park, H.-S. Min and R. W. Dutton: IEEE Electron Device Lett. **15** (1994) 348.
14. P. Scrobohaci and T.-W. Tang: IEICE Trans. Electron. **E77-C** (1994) 134.
15. R. Thoma, H. J. Peifer and W. L. Engl: J. Appl. Phys. **69** (1991) 2300.
16. J. Bude and K. Hess: Phys. Rev. B **45** (1992) 10958.
17. Y. Kamakura, H. Mizuno, M. Yamaji, M. Morifuji, K. Taniguchi, C. Hamaguchi, T. Kunikiyo and M. Takenaka: J. Appl. Phys. **75** (1994) 3500.
18. N. Sano and A. Yoshii: J. Appl. Phys. **75** (1994) 5102.
19. R. Thoma and W. L. Engl: Simulation of Semicond. Devices & Processes **4** (1991) 185.
20. T. Kunikiyo, M. Takenaka, Y. Kamakura, M. Yamaji, H. Mizuno, M. Morifuji, K. Taniguchi and C. Hamaguchi: J. Appl. Phys. **75** (1994) 297.
21. Y. A. El-Mansy and A. R. Boothroyd: IEEE Trans. Electron Devices **24** (1977) 254.
22. T. Y. Chan, P. K. Ko and C. Hu: IEEE Electron Device Lett. **6** (1985) 551.
23. N. Goldsman and J. Frey: Solid-State Electron. **31** (1988) 1089.
24. C. Hu, S. C. Tam, F. C. Hsu, P. K. Ko, T. Y. Chan and K. W. Terrill: IEEE Trans. Electron Devices **32** (1985) 375.

TABLES

Table I. The impact ionization models and the parameters used in Fig. 8. The parameters, α_0 and E_c, were obtained from the $\log\alpha$-$1/E$ plot of Monte Carlo results in homogeneous electric fields by a least squares fit method. The parameters, $g_{\mathrm{ii}\,0}$ and ε_c, were obtained from the $\log(G_\mathrm{ii}/n)$-$1/\langle\varepsilon\rangle$ plot by the same procedure.

Models	Formulas and Parameters
Local Field (LF)	$\alpha = \alpha_0 \exp\left(-\frac{E_\mathrm{c}}{E}\right)$ $\alpha_0 = 1.40 \times 10^6\ \mathrm{cm}^{-1}$, $E_\mathrm{c} = 1.32 \times 10^6\ \mathrm{V/cm}$
Non-Local Field (NLF)	$\alpha = \alpha_0 \exp\left(-\frac{d}{\lambda_\mathrm{p}}\right)$ $V_\mathrm{I} = \int_{x-d}^{x} \boldsymbol{E}\cdot d\boldsymbol{l},\ \lambda_\mathrm{p} = V_\mathrm{I}/E_\mathrm{c}$ $V_\mathrm{I} = 1.75$ eV[5]
Local Energy (LE)	$G_\mathrm{ii} = n g_{\mathrm{ii}\,0} \exp\left(-\frac{\varepsilon_\mathrm{c}}{\langle\varepsilon\rangle}\right)$ $g_{\mathrm{ii}\,0} = 1.39 \times 10^{14}\ \mathrm{s}^{-1}$, $\varepsilon_\mathrm{c} = 8.78$ eV
New Model	$G_\mathrm{ii} = n g_{\mathrm{ii}\,0} \exp\left(-\frac{\varepsilon_\mathrm{c}}{\langle\varepsilon\rangle_\mathrm{eff}}\right)$ $\langle\varepsilon\rangle_\mathrm{eff} = \langle\varepsilon\rangle \exp(\gamma(\xi - \xi_\mathrm{h}))$ $\gamma = \begin{cases} 4.2 & (\xi < \xi_\mathrm{h}) \\ 1.6 & (\xi > \xi_\mathrm{h}) \end{cases},$ $\xi_\mathrm{h} = 0.88$

FIGURES

Fig. 1. Calculated results in a homogeneous electric field, E, using Monte Carlo simulation. (a) The average energy of electrons, $\langle\varepsilon\rangle$. (b) The normalized average square energy of electrons, $\xi \equiv \sqrt{(3/5)\langle\varepsilon^2\rangle}/\langle\varepsilon\rangle$. The value of ξ converges to $\xi_{\rm h} = 0.88$ in a high field.

Fig. 2. Distribution functions for electrons in a homogeneous electric field. Solid lines are from Monte Carlo simulation. (a) Dashed lines are from eq. (6). (b) Dashed lines show Maxwell-Boltzmann distribution of the temperature defined by $3/2kT = \langle\varepsilon\rangle$. In both (a) and (b), $\langle\varepsilon\rangle$ and $\langle\varepsilon^2\rangle$ from the results of Monte Carlo simulation are used to calculate the distribution functions shown as dashed lines.

Fig. 3. Monte Carlo simulation result in an inhomogeneous electric field. (a) The electric field profile ncreases exponentially ($E = E_{\rm min}\exp(x/\lambda)$, $\lambda = 0.1\mu$m) and decreases linearly ($E = E_{\rm max} - a(x - x_{\rm max})$, $a = 1.0$kV$/\mu$m^2). The minimum electric field $E_{\rm min} = 1$kV/cm. $E_{\rm max}$ is the maximum electric field and $x_{\rm max}$ is its position. (b) The average energy. (c) The normalized average square energy.

Fig. 4. Distribution functions for electrons in the inhomogeneous electric field shown in Fig. 3. Solid lines are from Monte Carlo simulation, dashed lines are from eq. (17). $\langle\varepsilon\rangle$ and $\langle\varepsilon^2\rangle$ used in eq. (17) were calculated using the Monte Carlo simulator. (a) Point A ($x = 0.605\mu$m), (b) point B ($x = 0.655\mu$m), (c) point C ($x = 0.685\mu$m).

Fig. 5. Impact ionization rate as a function of inverse average electron energy. Solid line indicates the data calculated based on eqs. (17) and (18). Dashed line represents the Monte Carlo result in a homogeneous field.

Fig. 6. The effective energy for impact ionization given in eq. (21). The effective energy is calculated from the generation rate shown in Fig. 5. The dashed line indicates $\langle\varepsilon\rangle_{\rm eff} = \langle\varepsilon\rangle$. In the case of $\xi < \xi_{\rm h}$, the effective energy is lower than the average energy, meaning a lower generation rate compared to the homogeneous case. For $\xi > \xi_{\rm h}$, the effective energy is larger and, therefore, the generation rate is enhanced.

Fig. 7. The ratio of the effective energy, $\langle\varepsilon\rangle_{\rm eff}$, to the average energy, $\langle\varepsilon\rangle$, as a function of the normalized average square energy, ξ. The solid circles are from a least squares fit to the data in Fig. 6. The dashed lines are obtained from a least squares fit to the solid circles in the ranges of $\xi - \xi_{\rm h} < 0$, and $\xi - \xi_{\rm h} > 0$.

Fig. 8. Impact ionization rate in the inhomogeneous electric field shown in Fig. 3. The impact ionization models used are local field (LF), non-local field (NLF), local energy (LE), and new model (Present Work). Calculated result based on Monte Carlo (MC) simulation is also shown for comparison.

Fig. 9. Impact ionization rate in the inhomogeneous electric field. The field profile is similar to that in Fig. 3, except for the values of the parameters ($\lambda = 0.05\mu$m and $a = 1.5$kV/μm^2). The impact ionization models used are the same as in Fig. 8. (a) Electric field. (b) Impact ionization generation rate normalized by the electron concentration.

Fig. 10. Distribution functions for electrons in the inhomogeneous electric field shown in Fig. 9 ($\lambda = 0.05\mu$m). Solid lines are from Monte Carlo simulation, dashed lines are from eq. (17). $\langle\varepsilon\rangle$ and $\langle\varepsilon^2\rangle$ used in eq. (17) were calculated using the Monte Carlo simulator. (a) Point A ($x = 0.303\mu$m), (b) point B ($x = 0.323\mu$m), (c) point C ($x = 0.363\mu$m).

Fig. 11. Impact ionization rate in an inhomogeneous electric field. The field profile is similar to that in Fig. 3 except for the values of the parameters ($\lambda = 0.02\mu$m and $a = 2.5$kV/μm^2). The impact ionization models used are the same as in Fig. 8. (a) Electric field. (b) Impact ionization generation rate normalized by the electron concentration.

Fig. 12. Distribution functions for electrons in the inhomogeneous electric field shown in Fig. 11 ($\lambda = 0.02\mu$m). Solid lines are from Monte Carlo simulation, dashed lines are from eq. (17). $\langle\varepsilon\rangle$ and $\langle\varepsilon^2\rangle$ used in eq. (17) were calculated using the Monte Carlo simulator. (a) Point A ($x = 0.123\mu$m), (b) point B ($x = 0.143\mu$m), (c) point C ($x = 0.163\mu$m).

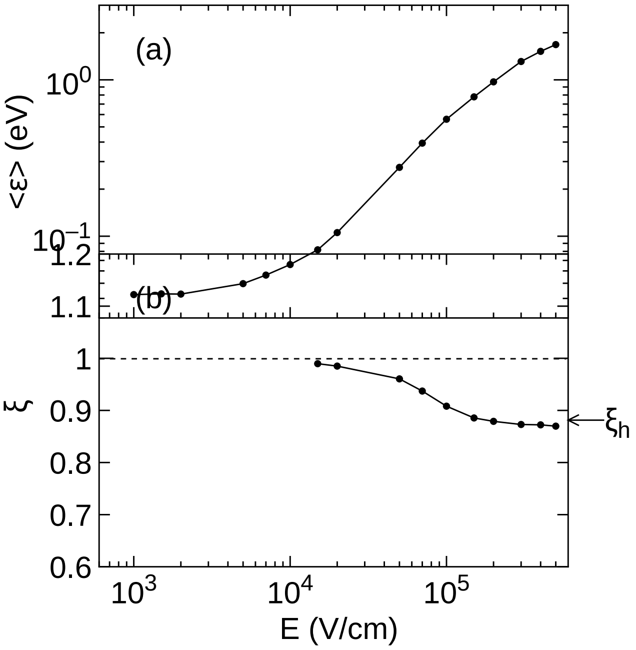
(a)
(b)
<ε> (eV)
10^0
10^{-1}
1.2
1.1
ξ
1
0.9
0.8
0.7
0.6
ξ_h
10^3
10^4
10^5
E (V/cm)

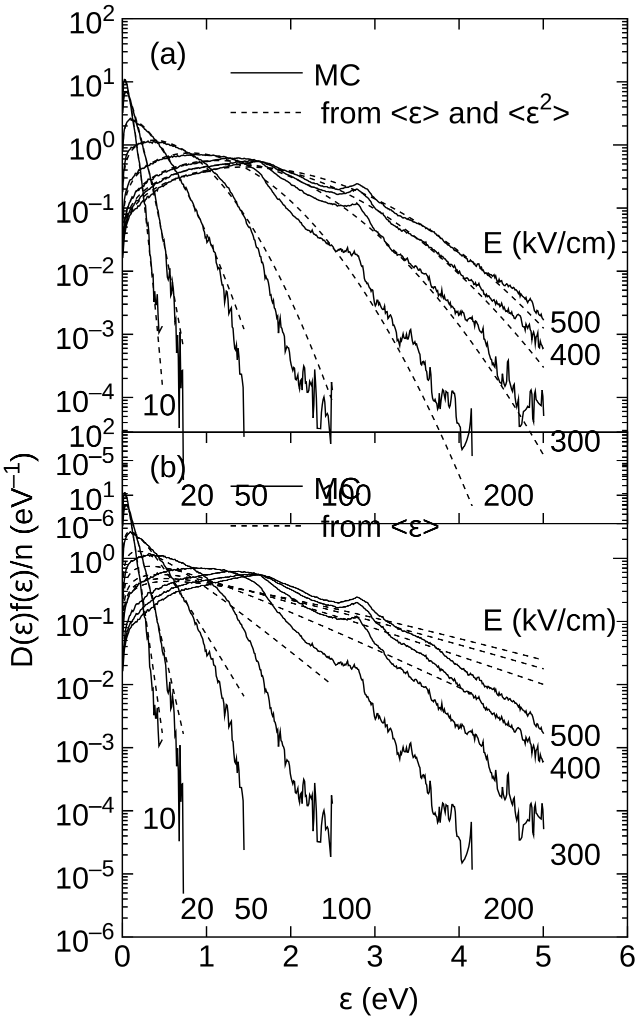
(a)
MC
from <ε> and <ε^2>
E (kV/cm)
10
20
50
100
200
300
400
500
(b)
MC
from <ε>
E (kV/cm)
10
20
50
100
200
300
400
500
D(ε)f(ε)/n (eV^{-1})
ε (eV)
10^2
10^1
10^0
10^{-1}
10^{-2}
10^{-3}
10^{-4}
10^{-5}
10^{-6}
0
1
2
3
4
5
6

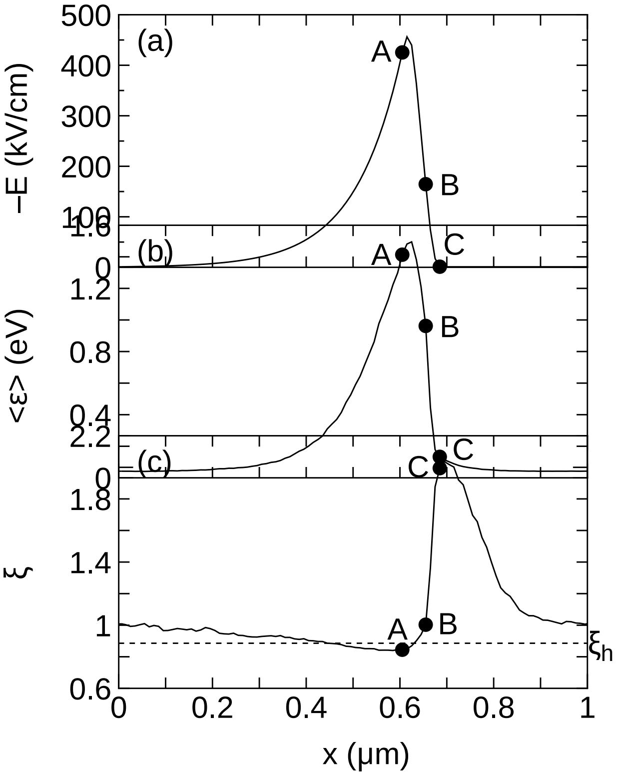

(a)
(b)
(c)
−E (kV/cm)
500
400
300
200
100
0
<ε> (eV)
1.6
1.2
0.8
0.4
0
ξ
2.2
1.8
1.4
1
0.6
A
B
C
ξ_h
0
0.2
0.4
0.6
0.8
1
x (μm)

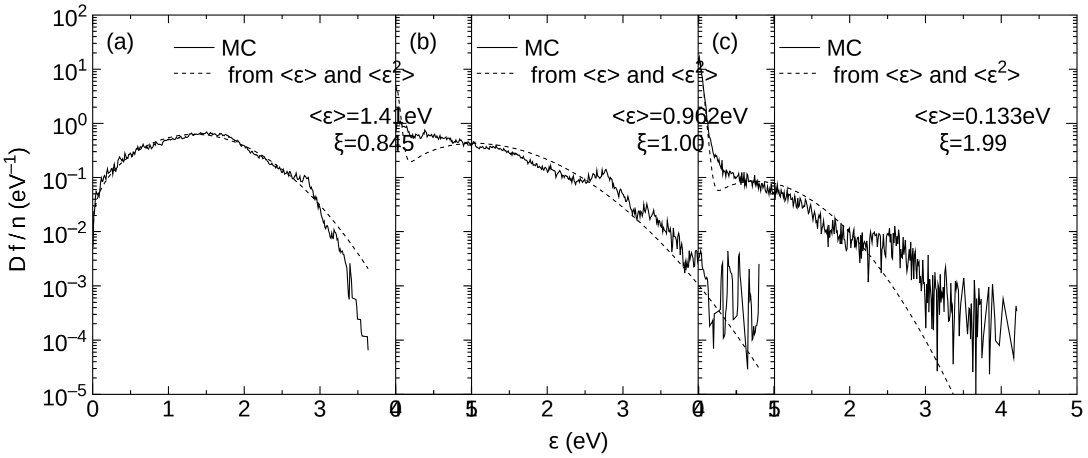
(a)
(b)
(c)
MC
from <ε> and <ε^2>
<ε>=1.41eV
ξ=0.845
<ε>=0.962eV
ξ=1.00
<ε>=0.133eV
ξ=1.99
D f / n (eV^{-1})
ε (eV)
10^2
10^1
10^0
10^{-1}
10^{-2}
10^{-3}
10^{-4}
10^{-5}
0
1
2
3
4
5

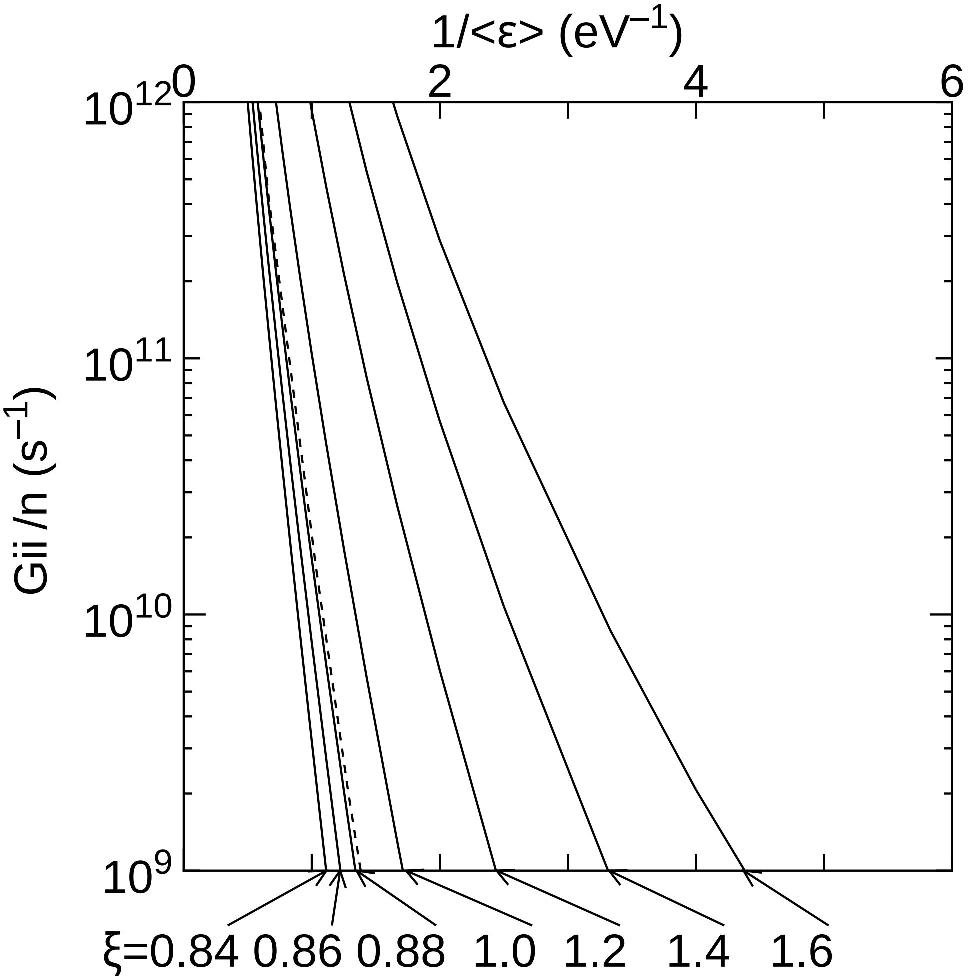
1/<ε> (eV^{-1})
0
2
4
6
10^{12}
10^{11}
10^{10}
10^{9}
Gii /n (s^{-1})
ξ=0.84
0.86
0.88
1.0
1.2
1.4
1.6

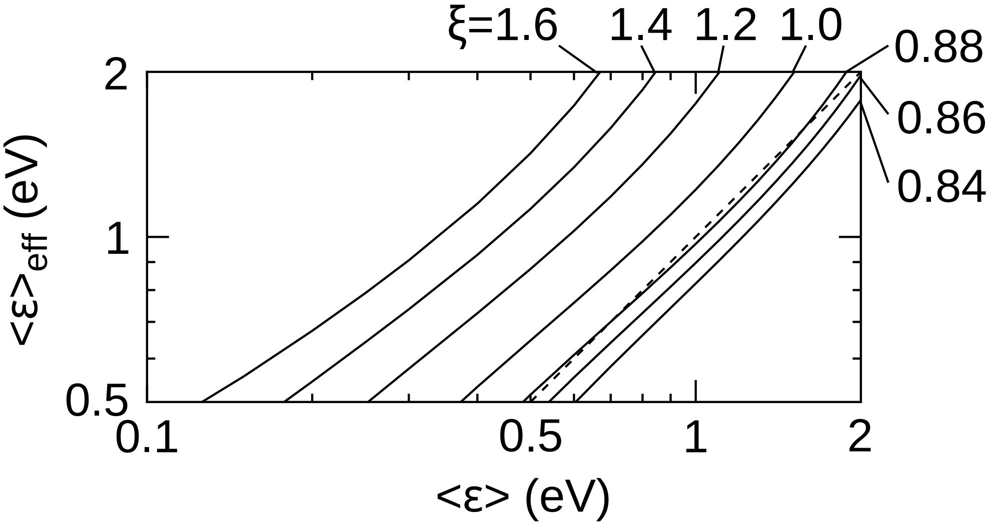
ξ=1.6
1.4
1.2
1.0
0.88
0.86
0.84
2
1
0.5
0.1
0.5
1
2
<ε>$_{eff}$ (eV)
<ε> (eV)

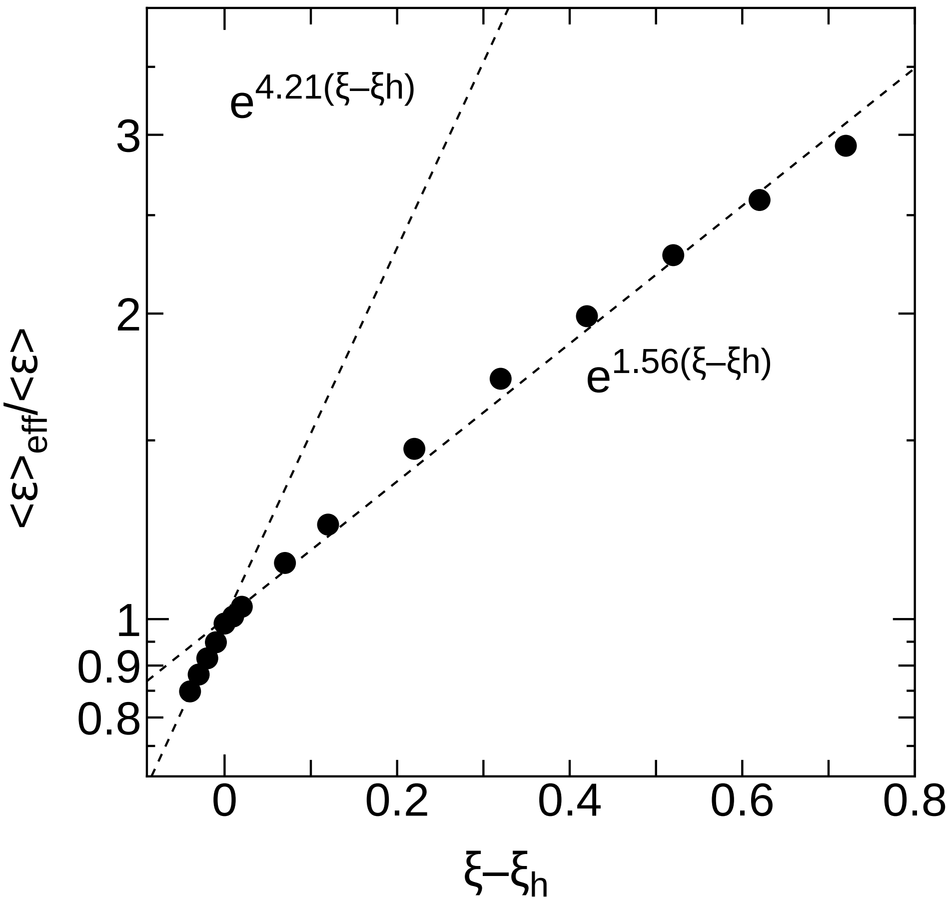
$e^{4.21(\xi-\xi h)}$
$e^{1.56(\xi-\xi h)}$
$\langle\varepsilon\rangle_{eff}/\langle\varepsilon\rangle$
$\xi-\xi_h$
0.8
0.9
1
2
3
0
0.2
0.4
0.6
0.8

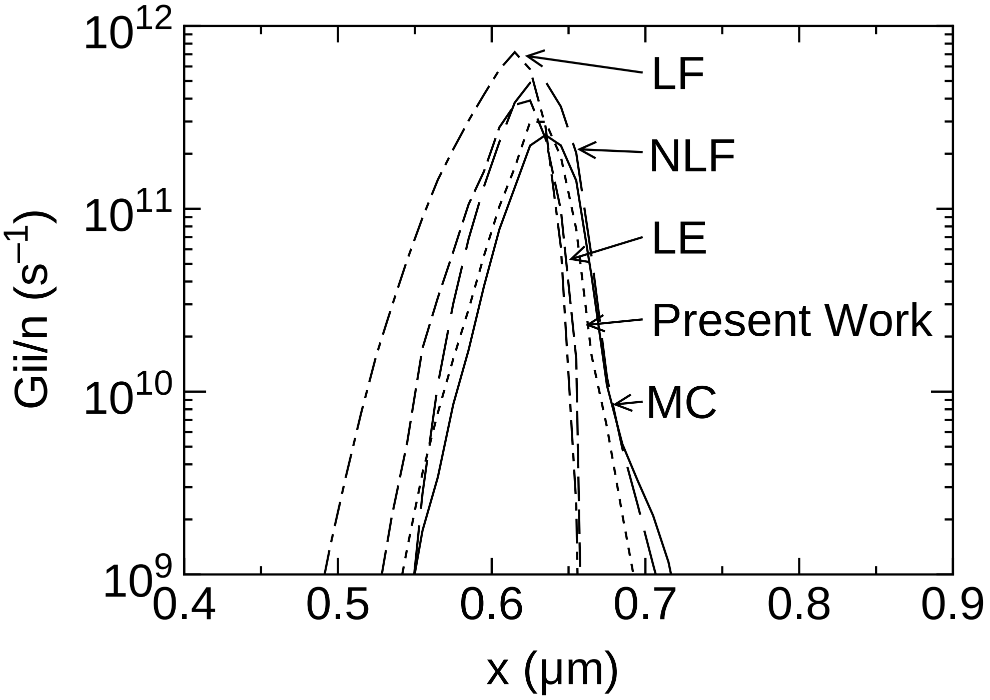
10^{12}
10^{11}
10^{10}
10^{9}
Gii/n (s^{-1})
0.4
0.5
0.6
0.7
0.8
0.9
x (µm)
LF
NLF
LE
Present Work
MC

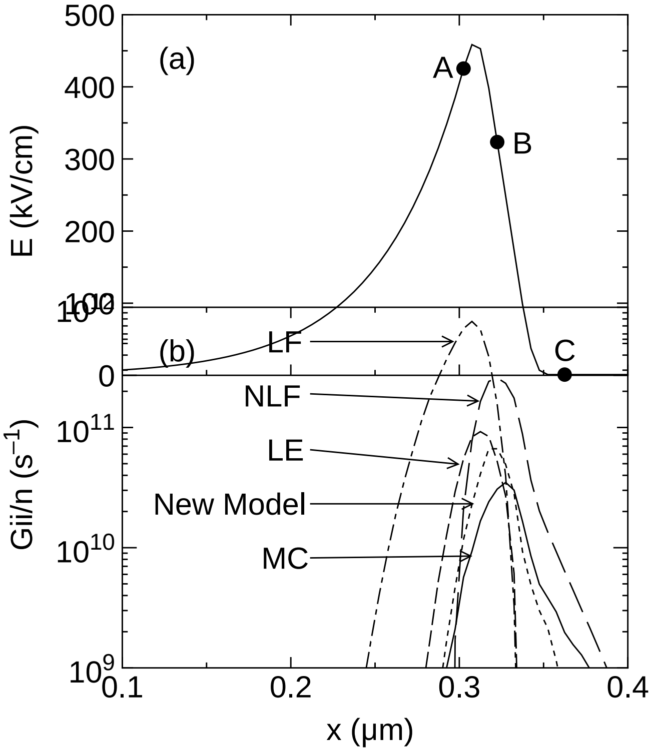
500
400
300
200
100
E (kV/cm)
(a)
A
B
C
10^{12}
LF
(b)
0
NLF
10^{11}
LE
New Model
10^{10}
MC
10^{9}
Gii/n (s^{-1})
0.1
0.2
0.3
0.4
x (µm)

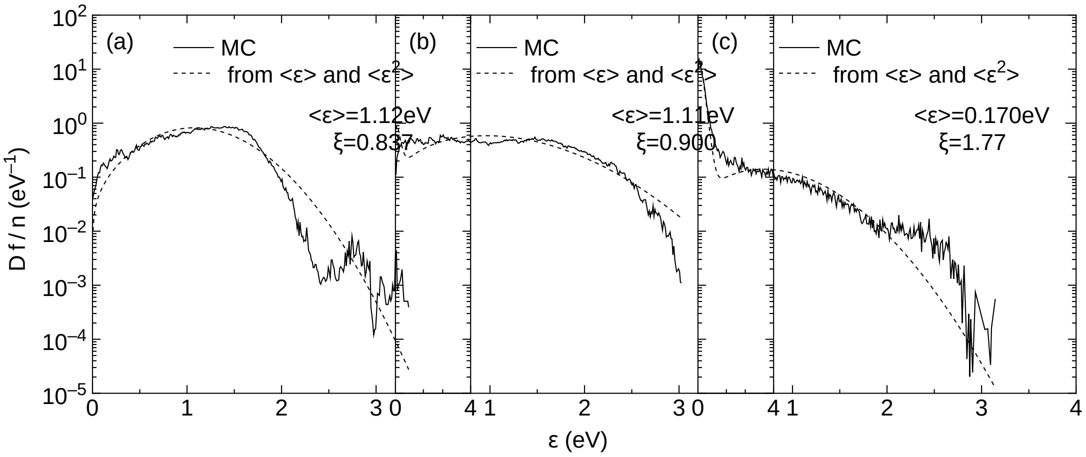
(a)
MC
from <ε> and <ε²>
<ε>=1.12eV
ξ=0.837
(b)
MC
from <ε> and <ε²>
<ε>=1.11eV
ξ=0.900
(c)
MC
from <ε> and <ε²>
<ε>=0.170eV
ξ=1.77
D f / n (eV⁻¹)
10²
10¹
10⁰
10⁻¹
10⁻²
10⁻³
10⁻⁴
10⁻⁵
0
1
2
3
4
ε (eV)

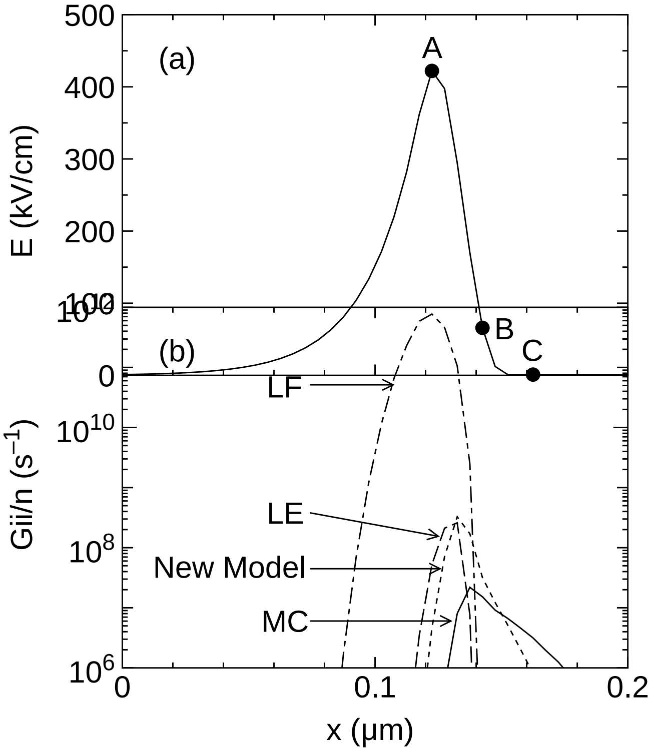
(a)
A
B
C
E (kV/cm)
500
400
300
200
100
0
(b)
10^{12}
10^{10}
10^{8}
10^{6}
Gii/n (s^{-1})
LF
LE
New Model
MC
0
0.1
0.2
x (μm)

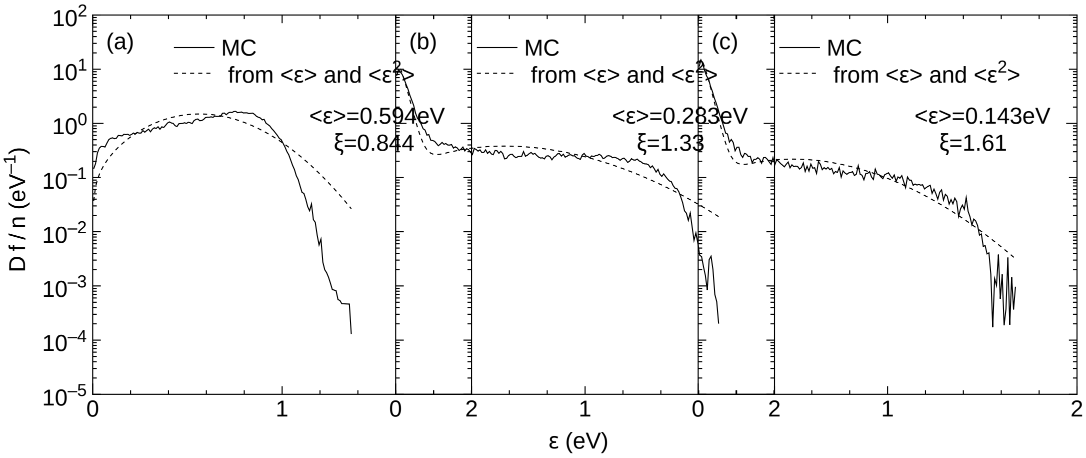
(a)
(b)
(c)
MC
from <ε> and <ε²>
<ε>=0.594eV
ξ=0.844
<ε>=0.283eV
ξ=1.33
<ε>=0.143eV
ξ=1.61
D f / n (eV⁻¹)
ε (eV)
10²
10¹
10⁰
10⁻¹
10⁻²
10⁻³
10⁻⁴
10⁻⁵
0
1
2